

# We are IntechOpen, the world's leading publisher of Open Access books Built by scientists, for scientists

6,900

Open access books available

186,000

International authors and editors

200M

Downloads

Our authors are among the

154

Countries delivered to

TOP 1%

most cited scientists

12.2%

Contributors from top 500 universities



WEB OF SCIENCE™

Selection of our books indexed in the Book Citation Index  
in Web of Science™ Core Collection (BKCI)

Interested in publishing with us?  
Contact [book.department@intechopen.com](mailto:book.department@intechopen.com)

Numbers displayed above are based on latest data collected.  
For more information visit [www.intechopen.com](http://www.intechopen.com)



---

# Graphene Field-Effect Transistor for Terahertz Modulation

---

Qi-Ye Wen, Yu-Lian He, Jing-Bo Liu, Qi Mao,  
Qing-Hui Yang, Zhi Chen and Huai-Wu Zhang

Additional information is available at the end of the chapter

<http://dx.doi.org/10.5772/intechopen.76744>

---

## Abstract

The real-world applications of terahertz (THz) technology necessitate versatile adaptive optical components, for example, modulators. In this chapter, we begin with a brief review on different techniques for THz modulation. After that, we introduce the extraordinary features of graphene along with its advantages and disadvantages as channel materials for field effect transistor (FET). We then discuss two types of graphene FET-based THz modulators, one is rigid and another is flexible. The feasibility of the high-quality THz modulators with different graphene FET structures has been successfully demonstrated. It is observed that by tuning the carrier concentration of graphene by electrical gating, the THz modulation can be obtained with relatively large modulation depth, broad width band, and moderate speed. This chapter helps the reader in obtaining guidelines for the proper choice of a specific structure for THz modulator with graphene FET.

**Keywords:** graphene, field effect transistor, terahertz, modulator, high-K dielectric layer, flexible

---

## 1. Introduction

The terahertz region of the electromagnetic spectrum roughly extends from 0.1 to 10 THz, corresponding to wavelengths from 3 mm to 30  $\mu\text{m}$ . Terahertz (THz) waves interact with a plethora of materials including solid state, chemical, and biological systems. Consequently, THz waves offer numerous applications including material characterization, imaging, wireless communication, and so on [1–4]. Such real-world applications of THz technology necessitate versatile adaptive optical components such as modulators, filters, lens, switches, waveguide,

polarizer, and so on. Among all these desired THz components and devices, modulators stand at on the focus of current interest [5]. Modulators can be used to control the amplitude, phase, polarization state, spatial propagation direction, pulse shape, and many more characteristic properties of electromagnetic waves and thus act as essential parts of sophisticated THz application systems such as wireless telecommunication or security imaging [6].

However, unlike the optical or microwave regime where active modulators are well established, the THz frequency regime is still in great demand for efficient, fast, and versatile active light modulators [6]. This is mainly due to the lack of natural materials that have tunable electromagnetic response to THz wave [5]. Nevertheless, materials including semiconductors [7, 8], metamaterials [9–12], superconductors [13, 14], and phase-transition materials [15, 16] have been intensively explored to control and manipulate THz wave with great progress being made in this direction. Modulators can be categorized by the technique or material system, which is employed to modulate the wave, for example, optical, electronic, thermal, and magnetic modulators.

The all-optical approach is an effective and attractive method to fabricate THz modulators, especially those with broadband or spatial operating features. Semiconductors, especially high-resistive (HR) silicon, have proven to be suitable for all-optical modulation of THz wave by converting photons into electrons upon optical illumination [17]. Generally, the pump laser produces a temporary region of high absorption or reflectance on semiconductor. THz wave, co-projected on this area, is thus modulated [18]. As a result, all optical spatial THz modulators, based on a bare silicon wafer, have previously been proposed to realize photo-designed THz devices [19] or reconfigurable quasi-optical THz components [20, 21]. Si is an attractive candidate for optical opponents because it is earth abundant, chemically stable, and has a suitable band gap. Silicon-based THz devices are particularly desirable as they would enable interfacing with existing and emerging Si-based optoelectronics, thereby providing potential low-cost route toward applications. However, a silicon wafer exhibits strong reflection to both optical light (~40%) and THz radiation (~30%), which greatly limits the achievable tunability and versatility. Xie et al. verified that the modulation depth (MD) of silicon wafer to THz wave is only 19.9% under 800 mW femtosecond laser, although this value could be 98.6% if the pump laser intensity is high enough [21]. Very recently, plasmonic layers [22], graphene [23, 24], and even thin organic layers [25] have been fabricated on the surface of Si to enhance the modulation properties. Si modulators with these additional layers can work under lower pumping power, while having the same or even two to four times larger modulation depth. Very recently, Qi-Ye Wen and his co-workers demonstrated an interesting Si nanostructure for optically driven THz modulators [26]. They showed that nanotip (SiNT) arrays made from silicon wafer can be utilized as antireflection layers for both THz wave and visible light to achieve a low-loss and spectrally broadband THz modulator with a remarkably enhanced MD. Instead of fabricating heterogeneous materials on silicon, the nanotips are directly etched from the Si substrate and thus are structurally stable. Compared with the modulators fabricated on bare silicon, a nearly three times larger MD is achieved with the SiNT modulator. Crucially, the intrinsic THz transmission of the SiNT modulator is as high as 90% due to a strong antireflection effect arising from the nanotip layer as a result of the formation of graded refractive index on the Si surface.

One disadvantage of the semiconductor-based all-optical THz modulators is its relatively low modulation speed. The ultimate modulation speed is decided by the carrier recombination

time of semiconductors, which for intrinsic or HR silicon is beyond 10  $\mu\text{s}$ , limiting the modulation speed to a maximum of  $\sim 100$  kHz. Though gallium arsenide (GaAs) has very short carrier lifetime (10–100 ps), it requires high-power pulsed laser excitation up to 1  $\text{kW}/\text{cm}^2$  to achieve similar results as Si [27]. The reason for this is that the carrier lifetime of semiconductor affects the modulation depth and speed in an opposite way. Further research is ongoing to overcome this problem [27].

Another method of THz modulation is to thermally tune the electrical conductivity and thus the optical response of semiconductors or metal oxides, especial those materials with insulator-metallic phase transition [15, 28–31]. Vanadium dioxide ( $\text{VO}_2$ ), for example, is a typical phase transition material that exhibits a reversible first-order phase transition from an insulating state to a metallic state above room temperature ( $\sim 68^\circ\text{C}$ ). Associated with this metal-insulator transition (MIT) is a lattice structural transition from the monoclinic to tetragonal, a change of conductivity by 3–5 orders of magnitude and significant changes of the optical properties at all wavelengths. Since the insulated state is transparent while conductive state is opaque to THz wave, the THz transmission can thus be dynamically modified from transparent to reflecting modes by controlling the phase transition of the  $\text{VO}_2$  film.  $\text{VO}_2$  films, separately or integrated with resonant element (e.g., metamaterials), have already been used to control and manipulate THz wave [15, 30, 32, 33].

Although great progress has been made in optically and thermally driven THz modulators, an all-electronic approach is more interesting and attractive for the real application. It is well known that the carrier concentration in semiconductors can be tuned by electric injection or depletion of charge carriers. It is proved that THz wave can be manipulated by the use of two-dimensional electron gases (2DEGs) in semiconductors [7, 8]. A semiconductor-based field-effect transistor (FET) is a very useful architecture to fabricate effective THz modulators.

## 2. Graphene and graphene field-effect transistors

Graphene is a quasi-two-dimensional isolated monolayer of carbon atoms that are arranged in a hexagonal lattice. It is well known for its remarkable electron mobility at room temperature, with reported values in excess of  $15,000 \text{ cm}^2 \cdot \text{V}^{-1} \cdot \text{s}^{-1}$  [34]. Hole and electron mobilities were expected to be nearly identical. Graphene holds great promise for various material/device applications, including solar cells [35], light-emitting diodes (LED), touch panels, and smart windows or phonesal [36].

Graphene is a zero-band-gap semiconductor where conduction and valence bands meet at the Dirac points. The band gap is an extremely important characteristic of the semiconductor for transistor application, which enables the transistor device to turn off and minimizes leakage current at off state. In this circumstance, the gapless band structure of single-layer graphene makes it unsuitable for the direct use of graphene-based field-effect transistors (FET), though it is one of the most widely discussed applications in electronics. In order to overcome the challenges faced in incorporating graphene into microelectronic applications, great efforts have gone into developing three main aspects including developing a synthesis technique to manufacture graphene over wafer-scale areas, forming a high-quality gate dielectric on the surface of graphene, and, most importantly, opening an energy band gap in graphene. This

results in the observation that narrow ribbon widths down to less than 10 nm are required to open a band gap in graphene and achieve an acceptable level of low off currents. However, fabricating of narrow ribbons of that dimension is a big challenge even with current advanced lithographic techniques [37, 38].

The zero-band-gap characteristic means that the density of states (DOS) in graphene is linear with respect to the energy level. Therefore, gate voltage can modulate the DOS linearly to enable modulation of carrier (current) in the channel. In other words, graphene-based field-effect transistor (GFET) can be used to tune the carrier concentration in graphene by applying a voltage at the gate, making it possible to modulate the absorption/transmission of THz wave through the devices. Recently, such a graphene-based THz modulator was demonstrated by Sensale-Rodriguez et al. and Maeng et al. [39, 40]. It is reported that the transmission of THz wave through graphene can be controlled by electrically tuning the density of states available for intra-band transitions. Though the modulation depth and speed are limited to 15% and 20 kHz by this electrical device prototype, it opens a new direction for graphene application in a transistor structure [39, 40].

### 3. Enhanced GFET THz modulator with high-k dielectric layer

In most GFET devices, ~300-nm  $\text{SiO}_2$  was used as the gate dielectric on top of a p-type silicon (p-Si) substrate. However, when used as a THz broadband modulator, GFET with graphene/~300 nm  $\text{SiO}_2$ /p-Si structures has drawbacks such as high switching voltage, small modulation depth, and slow modulation speed [39, 40]. Alternatively,  $\text{Al}_2\text{O}_3$  with a dielectric constant of 7.5 is a high- $\kappa$  material with numerous outstanding dielectric properties in comparison with  $\text{SiO}_2$  [41]. In this chapter, we introduce a high-efficiency broadband THz wave modulator with quicker modulation speed and larger modulation depth by using  $\text{Al}_2\text{O}_3$ -based large-area graphene GFET device. The modulator consists of graphene monolayer/~60 nm  $\text{Al}_2\text{O}_3$ /p-Si structures. In our device, an intensity modulation depth of 22% (1% per 1.36 V) and a modulation speed of 170 kHz have been successfully achieved, which are notable improvements from previously reported 15% and 20 kHz, respectively, in the broadband modulators with graphene/~95 nm  $\text{SiO}_2$ /Si structures [39].

#### 3.1. Fabrication and characteristics of the enhanced THz modulator

The native oxide layer on the (100) p-Si ( $\rho \sim 1\text{--}10 \Omega\text{-cm}$ ) substrate was dissolved by buffered oxide etching solution to make a naked hydrophobic silicon surface. An  $\text{Al}_2\text{O}_3$  film was deposited on top of the silicon substrate by atomic layer deposition (ALD) technique at 120°C using trimethylaluminum (TMA) and  $\text{O}_2$  as the source [42]. **Figure 1(a)** shows the X-ray diffraction (XRD) of the  $\text{Al}_2\text{O}_3$  thin film on Si substrate scanned by the Cu  $K\alpha$  radiation. The strong peak at  $69^\circ$  is attributed to the silicon substrate, and the sharp peak at  $\sim 33^\circ$  coincides with the reflection of the  $\alpha\text{-Al}_2\text{O}_3$  phase, which indicates that the  $\text{Al}_2\text{O}_3$  film is a single crystalline. **Figure 1(b)** shows the cross-section of the sample characterized by scanning electron microscope (SEM). As shown in **Figure 1(b)**, the deposited  $\text{Al}_2\text{O}_3$  layer is dense and smooth with a thickness of ~60 nm. Both XRD spectrum and SEM image confirm that  $\text{Al}_2\text{O}_3$  films were well prepared by the ALD system.

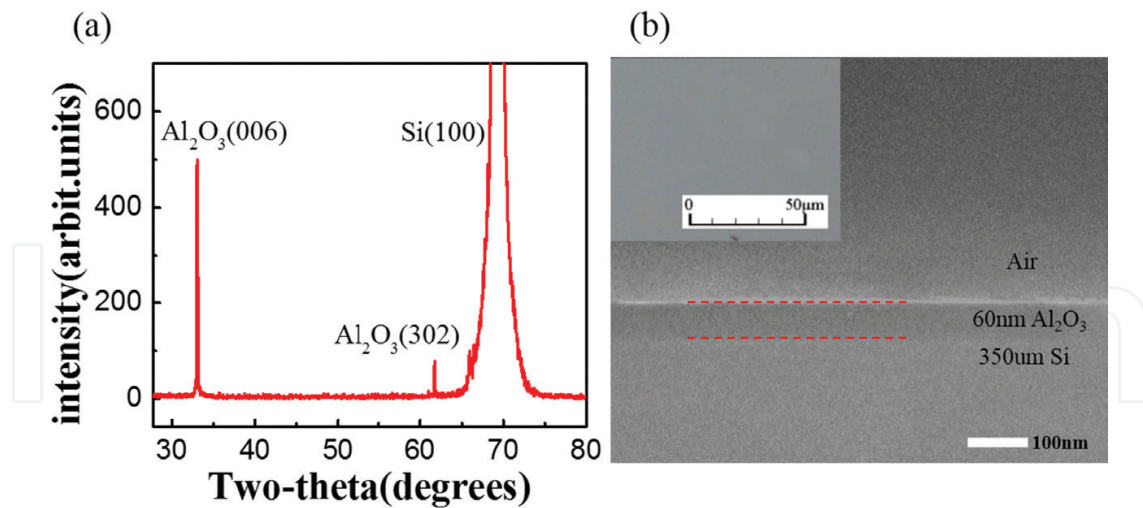


**Figure 1.** (a)  $\theta$ - $2\theta$  scan of Al<sub>2</sub>O<sub>3</sub>-based GFET by X-ray diffraction with CuK $\alpha$  radiation and (b) SEM image of the cross-section of a single crystalline ~60 nm Al<sub>2</sub>O<sub>3</sub> film on the Si substrate. The inset shows the surface of graphene/Al<sub>2</sub>O<sub>3</sub> obtained by optical microscope. The dash lines are a guide to the eye.

Large-area monolayers of graphene films were synthesized by chemical vapor deposition (CVD) on a copper foil, which were then transferred onto the ~60-nm Al<sub>2</sub>O<sub>3</sub>/p-Si substrate and 300-nm SiO<sub>2</sub>/p-Si substrate, respectively [43, 44]. The SiO<sub>2</sub>/p-Si substrate was used to fabricate the reference sample. The transferred graphene monolayers on the Al<sub>2</sub>O<sub>3</sub>/p-Si and SiO<sub>2</sub>/p-Si substrate were characterized by a Raman spectroscopy with a 514 nm laser in **Figure 2(a)**. The two obvious peaks in the Raman spectra of graphene on the Al<sub>2</sub>O<sub>3</sub>/p-Si substrate are the G peak at ~1591 cm<sup>-1</sup> and two-dimensional peak at ~2687 cm<sup>-1</sup>. The peak intensity ratio  $I_G/I_{2D}$  is ~0.43, and the full-width at half-maximum (FWHM) of the two-dimensional peak is about 38 cm<sup>-1</sup>. In addition, the intensity of the D peak at 1341 cm<sup>-1</sup> is low with an  $I_D/I_G$  ratio of ~0.18, indicating that the transferred graphene is a high-quality monolayer which is similar to the sample grown on the SiO<sub>2</sub>/p-Si substrate [45, 46]. The optical microscope shows the top view of the graphene/Al<sub>2</sub>O<sub>3</sub> in the inset of **Figure 1(b)**, confirming that the device surface is smooth, uniform, and free of pinholes over large areas.

To acquire further understanding of the THz modulation characteristics, we now discuss the carrier properties of the graphene layer under electrical biasing. As graphene can be treated as a thin film, the frequency-dependent amplitude transmission  $|T(\omega)|$  is given by  $|T(\omega)| = \left| \frac{1}{1 + NZ_0 \sigma(\omega)/(1 + n_s)} \right|$ , where  $N = 1$  is the number of graphene layer,  $Z_0$  is the vacuum impedance, and  $n_s$  is the effective refractive index of the substrate.  $\sigma(\omega)$  is the complex sheet conductivity of graphene, which can be described by the simple Drude model, namely  $\sigma(\omega) = \frac{iD}{\pi(\omega + i\Gamma)}$ , where  $\Gamma$  is the carrier-scattering rate and  $D$  is the Drude weight.  $D$  can be further expressed as  $D = (V_F e^2/\hbar)(\pi|n|)^{1/2}$ , where  $V_F$  is the Fermi velocity,  $e$  is the electron charge,  $\hbar$  is the reduced Planck constant, and  $n$  is the carrier concentration of graphene. The corresponding variation of the  $E_F$  in graphene extracted from  $|E_F| = \hbar V_F(\pi|n|)^{1/2}$  clearly shows the relation between  $E_F$  and the carrier concentration  $n$ . **Figure 2(b)** shows the conical band structures of graphene, whose Fermi level and carrier concentration can be changed by applying different gate biases in a GFET. As a result, the transmittance of the THz wave could be modulated by varying the applied bias voltages at the gate. Ambient atmosphere and processing residual on the surface of graphene often deviates the Dirac point of graphene from the zero voltage point [47]. To tune the transmittance of

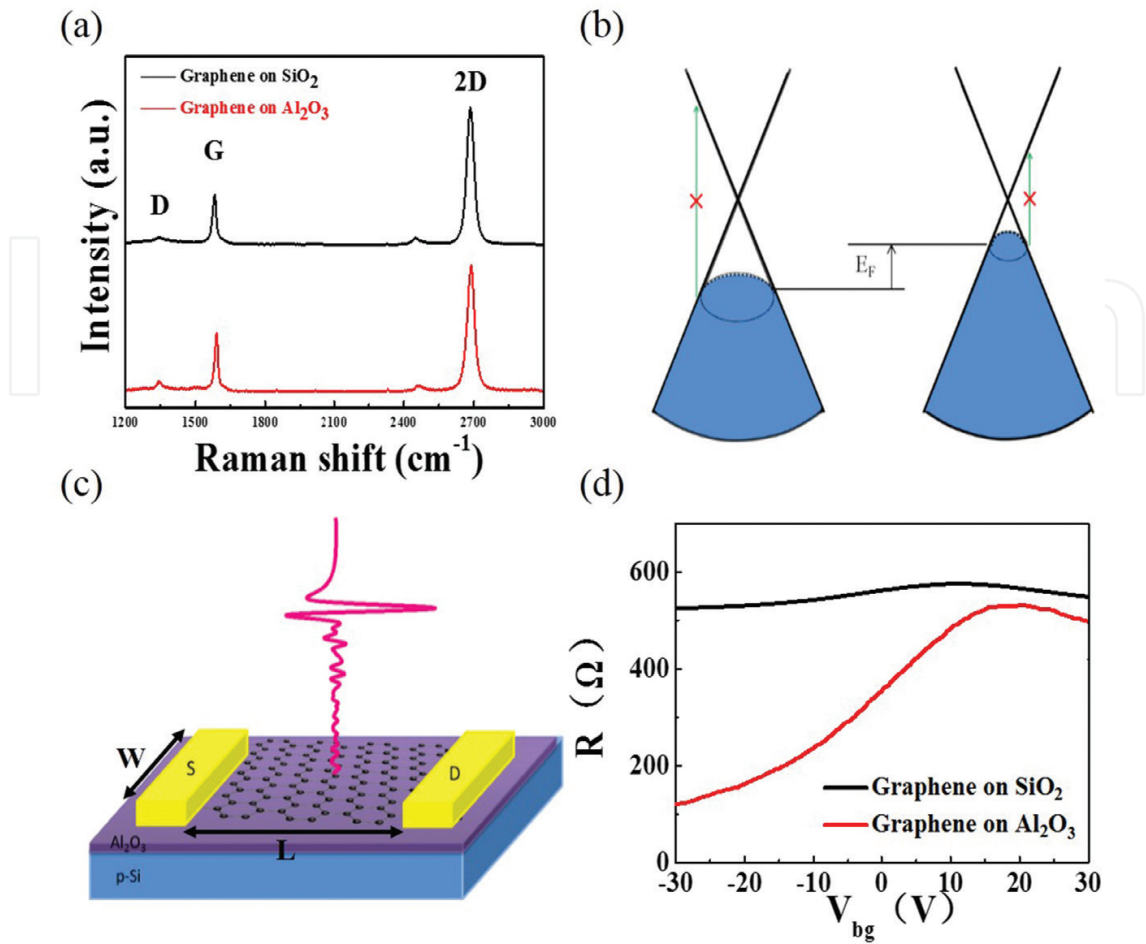


**Figure 2.** (a) Raman spectra of the monolayer graphene on the 300 nm SiO<sub>2</sub>/p-Si and 60 nm Al<sub>2</sub>O<sub>3</sub>/p-Si substrate. (b) conical band structure of graphene and the sweeping of the Fermi level. (c) the scheme of GFET and THz transmission ( $W = 5$  mm,  $L = 5$  mm). (d) Total resistance  $R_{total}$  as a function of back gate voltage  $V_{bg}$  in the GFET.

THz wave through the graphene, a bias at gate was applied to deviate  $E_F$  further from the charge neutrality point (CNP) where carrier density of state and thus  $\sigma_{DC}(E_F)$  and  $\sigma(\omega)$  are minimized due to the conical band structure.

In addition, to evaluate the CNP of monolayer graphene, a graphene-based FET based on Al<sub>2</sub>O<sub>3</sub>/p-Si was fabricated with silver paste as the source and drain electrodes, respectively. Meanwhile, p-Si was used as the back gate to vary the carrier concentration  $n$  and Fermi level  $E_F$  of graphene as shown in **Figure 2(c)**. Based on the transfer characteristic measurement, the resistance between source and drain ( $R_{total}$ )-dependent back gate voltage ( $V_{bg}$ ) is shown in **Figure 2(d)**. The maximum resistance of the graphene FET occurs at 18 V, where Fermi level is located at the CNP for this device. The Fermi level of graphene would tend to remain with CNP with the back-gate voltage closing to the Dirac voltage. Carrier concentration got the minimum and the THz transmittance got the maximum at the CNP, respectively. The fabrication of SiO<sub>2</sub>-based GFET is similar to that of the Al<sub>2</sub>O<sub>3</sub>-based devices. The CNP of SiO<sub>2</sub>-based GFET is ~15 V, which is very close to Al<sub>2</sub>O<sub>3</sub>-based devices.

The carrier mobility ( $\mu$ ) in GFET can be calculated by  $\mu = g_m L / (WC_g V_{ds})$ , where  $g_m = dI_{ds} / dV_{bg} |_{V_{ds} = \text{constant}}$  is obtained from the  $R_{total} - V_{bg}$  curve shown in **Figure 2(d)**; both of the length ( $L$ ) and width ( $W$ ) of graphene channel are 5 mm; the constant  $V_{ds}$  is 1 V; the back-gate capacitance

per unit area,  $C_g$  is 11.9 nF/cm<sup>2</sup> for SiO<sub>2</sub> GFET, and 110.625 nF/cm<sup>2</sup> for Al<sub>2</sub>O<sub>3</sub> GFET [48]. With these parameters the carrier mobility of graphene on Al<sub>2</sub>O<sub>3</sub> and SiO<sub>2</sub> were calculated to be 682.4 and 546.2 cm<sup>2</sup> V<sup>-1</sup> s<sup>-1</sup>, respectively. It can be seen that the carrier mobility of GFET on Al<sub>2</sub>O<sub>3</sub> is larger than that on SiO<sub>2</sub>. More importantly, the  $g_m$  of GFET on Al<sub>2</sub>O<sub>3</sub> (~75.5  $\mu$ S) is calculated to be 11 times higher than that on SiO<sub>2</sub> (~6.5  $\mu$ S) [41]. According to the equation, the huge difference in  $g_m$  indicates a large discrepancy in the back-gate capacitance ( $C_g$ ) and consequently in the carrier density variation for Al<sub>2</sub>O<sub>3</sub> and SiO<sub>2</sub>-based GFET. Due to the larger  $g_m$  and higher carrier mobility, a larger modulation depth and higher speed can be anticipated in Al<sub>2</sub>O<sub>3</sub>-based GFET modulator, respectively.

### 3.2. Modulation properties of the enhanced THz modulator

To further compare the THz modulation properties of devices on SiO<sub>2</sub>/p-Si and Al<sub>2</sub>O<sub>3</sub>/p-Si substrate, we applied to the modulators with back voltages ranging from -20 to 10 V with an increment of 5 V. A blank p-Si substrate was used as a reference sample to eliminate the substrate effect. The THz transmission spectra, we would discussed later, were all normalized to a blank p-Si substrate and the absorption from the substrate was also removed. Therefore, what we analyzed in the following is almost the intrinsic properties of the graphene itself.

We measured the spectral transmission of the modulators by a typical optical-fiber integrated terahertz time-domain spectroscopy (TDS). **Figure 3(a)** shows the normalized THz transmission intensity through a GFET with graphene/~300 nm SiO<sub>2</sub>/p-Si sandwich structures under each applied back voltage from -20 to 10 V and 0.4–1.5 THz. A weak modulation of the THz transmission indicates a small swing of graphene Fermi level under the back gate bias between 20 and -10 V. A specific frequency of 1 THz was chosen to discuss the modulation behaviors. The gate-dependent transmission curve exhibited a minimum transmission of 88% at -20 V and gradually reached a maximum of 90% at 10 V. The modulation depth was thus calculated by  $|(T(10\text{ V}) - T(-20\text{ V})) / T(10\text{ V})|$  to be ~2% (1% per 15 V). A thicker SiO<sub>2</sub> back-gate dielectric layer would increase the cavity effect along the transmission direction leading to the weaker modulation [39].

**Figure 3(b)** shows the modulation curves measured for Al<sub>2</sub>O<sub>3</sub>-based GFET. A distinctive variation in THz wave transmission was observed at a different gate voltage from -20 to 10 V. At 1 THz, the transmission exhibited a minimum of 71% at -20 V and reached a maximum of 91.3% at 10 V. The total modulation depth was calculated to be 22%. The amplitude of THz transmission is approximately flat from 0.4 to 1.5 THz at each gate voltage, indicating that the Al<sub>2</sub>O<sub>3</sub>-based GFET is an efficient broadband THz modulator. **Figure 3(c)** shows the extracted modulation depth of Al<sub>2</sub>O<sub>3</sub>-based GFET from 0.4 to 1.5 THz at different applied gate voltages. It is clear that the maximum modulation depth of 22.5% occurs at 0.85 THz with  $V_{bg} = -20$  V. The transmission of THz wave is primarily determined by carrier density, which in turn can be precisely tuned by  $V_{bg}$ . **Figure 3(d)** compares the transmitted amplitudes of THz wave at the frequency of 1 THz through the GFET with SiO<sub>2</sub> and Al<sub>2</sub>O<sub>3</sub> gate dielectric at different  $V_{bg}$ . As shown in **Figure 3(d)**, the modulation of THz wave transmission can be greatly improved by replacing the SiO<sub>2</sub> with Al<sub>2</sub>O<sub>3</sub> as dielectric materials in GFET.

The dynamic modulation characteristics of Al<sub>2</sub>O<sub>3</sub>-based modulator were further studied with a homemade setup, in which a Virginia Diodes (VDI) continuous-wave (CW) terahertz source with

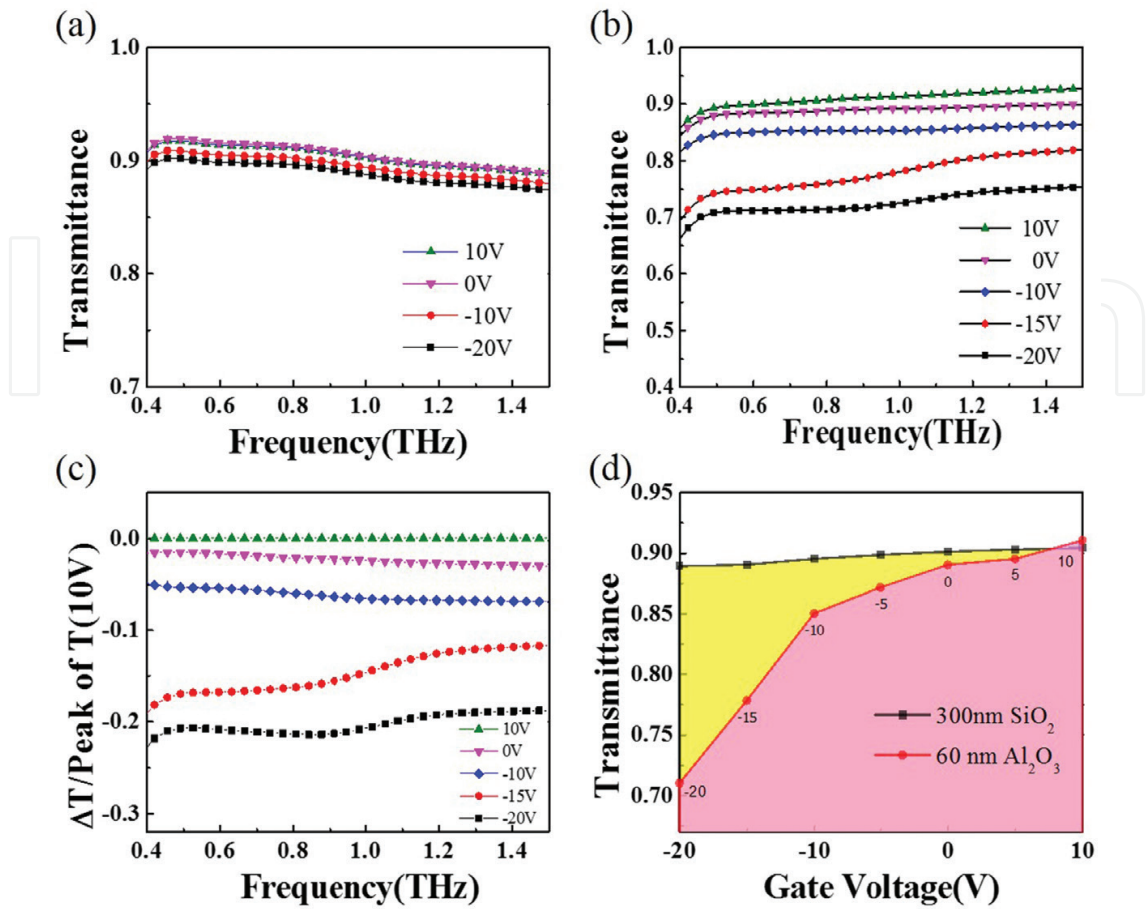


**Figure 3.** Normalized intensity of transmitted THz wave through the (a)  $\text{SiO}_2$ - and (b)  $\text{Al}_2\text{O}_3$ -based GFET at different back gate voltage. The modulation depth of  $\text{Al}_2\text{O}_3$ -based GFET as a function of applied gate voltage is shown in (c), and (d) the comparison of the amplitudes of the THz wave transmission through the GFET modulators with  $\text{SiO}_2$  and  $\text{Al}_2\text{O}_3$  dielectric at 1 THz.

a central output in the 340 and a 240–400 GHz zero-bias Schottky diode intensity detector are included. In the measurement, we applied a square biasing voltage to the device and the output modulated THz waveform was recorded by an oscilloscope. The applied voltage pulse is  $-10$  V at the minimum and  $10$  V at the maximum with various modulation frequencies. **Figure 4(a)** shows the recorded waveform of  $\text{Al}_2\text{O}_3$ -based modulator at a carrier frequency of  $340$  GHz. **Figure 4(b)** shows the dependence of the normalized modulation magnitude on the modulation frequency, which gives rise to a 3-dB bandwidth ( $f_c$ ) of  $170$  kHz. As we know, the RC time constant of a transistor is an important parameter to determine the switch speed. The device resistance ( $R$ ) was estimated to be  $261 \Omega$  by extracting the average resistance as the back voltage sweeping from  $-10$  to  $10$  V. The capacitance ( $C$ ) can be expressed by  $C = A\epsilon\epsilon_0/d$ , where  $\epsilon$  is the relative dielectric constant of the ALD-deposited  $\text{Al}_2\text{O}_3$  film ( $\sim 7.5$ ),  $\epsilon_0$  is the permittivity of free space,  $A$  is the effective area of active graphene device of  $5 \times 5 \text{ mm}^2$ ,  $d$  is thickness of the  $\text{Al}_2\text{O}_3$  film of  $60 \text{ nm}$ . The capacitance  $C$  is then calculated to be  $\sim 27.7 \text{ nF}$ . As a result, the calculated RC time constant is  $\sim 138.7 \text{ kHz}$ , which is very close to the directly measured 3-dB bandwidth ( $170 \text{ kHz}$ ). These results confirm that  $\text{Al}_2\text{O}_3$ -based GFET possesses a higher modulation speed than the conventional silicon-based graphene THz modulators [39].

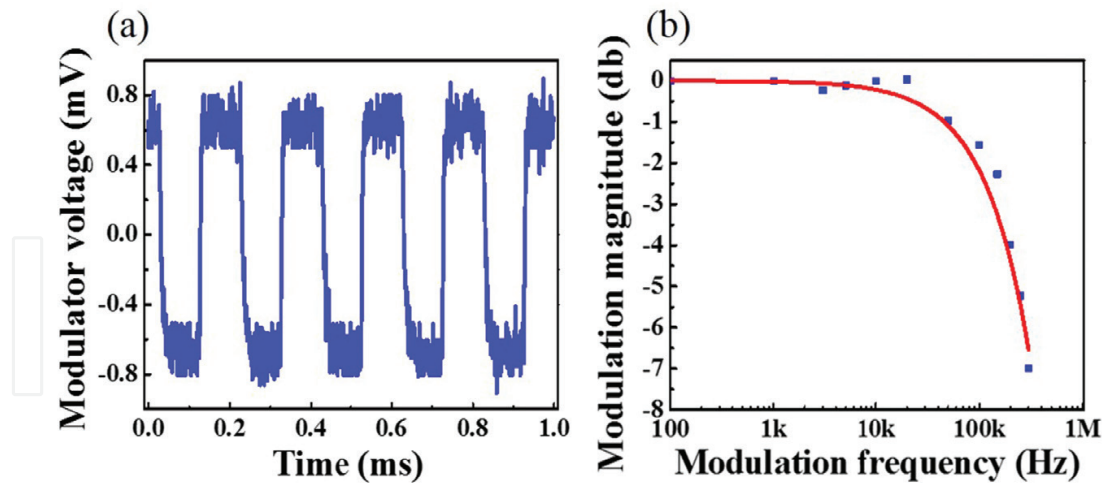


**Figure 4.** (a) Modulated THz waveform from the  $\text{Al}_2\text{O}_3$ -based modulator under a square voltage pulse at a modulation frequency of 5 kHz. (b) the dependence of the normalized modulation magnitude on the modulation frequency.

Obviously, the  $\text{Al}_2\text{O}_3$  film is superior over  $\text{SiO}_2$  as a gate dielectric in GFET modulator. By replacing 300 nm  $\text{SiO}_2$  with 60 nm  $\text{Al}_2\text{O}_3$ , an enhancement of 11 times in modulation depth was observed. Furthermore, the modulation speed increased from 20 to 170 kHz as well. One reason for this significant improvement is that the high- $\kappa$  dielectrics can remarkably reduce the Coulomb impurity scattering [41] to achieve a high  $g_m$  and consequently a larger THz modulation depth [49]. This work provides an effective method to fabricate high quality GFET THz wave modulator with large modulation depth and fast switch speed, which is vital for many THz technology applications as well as for fundamental research.

#### 4. Flexible THz modulator based on graphene FET

In contrast to rigid THz modulators, flexible THz modulators are expected to be used in application fields with complicate surfaces [50]. A typical type of flexible modulator is a field-grating device, with which the intensity or phase of THz wave can be modulated by electrical gating or laser, but its properties remain unchanged under device deformation. This device is highly desired in nonplanar applications. Graphene is a highly flexibility material where its electronic structure can be maintained under deformation. Therefore, it is promising to develop flexible THz modulators based on graphene FET. Here, we give a typical example.

##### 4.1. Device fabrication of the flexible THz modulator

The schematic diagram and photograph of the flexible THz modulator are presented in **Figure 5(a)** and **(b)**, respectively. The whole device is fabricated on a flexible commercial PET substrate. First, monolayer graphene was synthesized by typical chemical vapor deposition (CVD) on the copper foil and then was transferred onto the PET substrate [44–46]. The silver pastes were brushed at the two sides of graphene strip as the source and drain electrodes. The effective length and width of the channel of graphene FET was defined to be 2 and

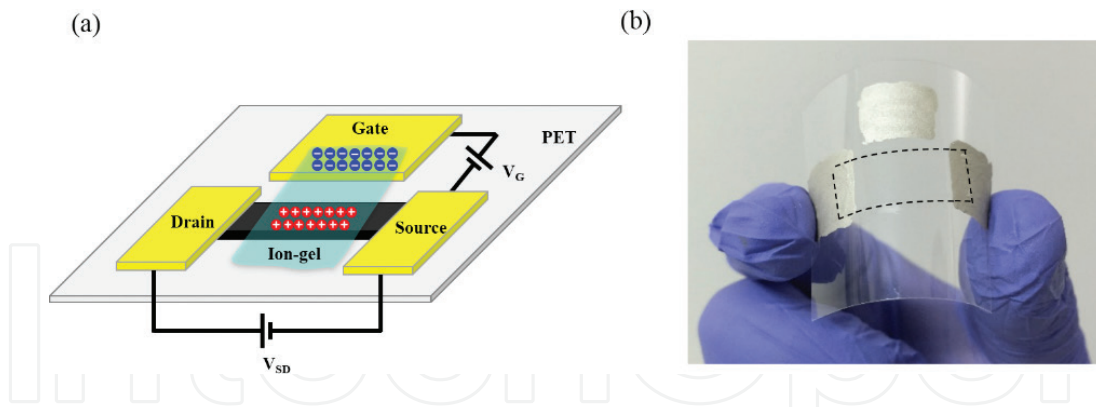


**Figure 5.** (a) Schematic structure of the flexible THz modulator based on graphene coplanar-gate FET. (b) Photograph of the flexible THz modulator in the bending condition, where the boundary of graphene channel is marked with dotted lines.

1 cm, respectively. The ion-gel, which is a mixture of lithium perchlorate, polyethylene oxide (PEO), and carbinol, was spin coated on the surface of the graphene as the gate dielectric. The work principle of this coplanar-gate FET structure is: when a positive voltage to the device is applied, as shown in **Figure 5(a)**, negative and positive ions in the ion-gel accumulate onto the gate electrode and graphene channel, respectively. A strong electric field is thus imposed to the graphene to modulate the carrier concentration and as a result a modulation to the THz radiation is realized.

#### 4.2. Modulation properties of the flexible THz modulator

The intensity modulation performance of flexible THz modulator has been investigated by using a homemade fiber-coupled THz-time domain spectroscopy (TDS). A pair of photoconductive antenna made on LT-InGaAs/InAlAs is used as both the emitter and detector, which prove a bandwidth of 2 THz approximately. The THz wave from the emitter is focused onto the center of the sample with a beam diameter of 3 mm, covering the active area of the modulator. In order to study the flexible performance of our THz modulator, the device has been measured in the flat, convex, and concave conditions, respectively. The bending strain is  $\sim 1\%$ , which is defined as  $\text{strain} \approx (t_s - t_p) / 2r_c$  ( $t_s, t_p \gg t_f$ ) [51].  $t_s$  is the thickness of the flexible PET substrate ( $\sim 125 \mu\text{m}$ ),  $t_p$  the thickness of the ion-gel ( $\sim 10 \mu\text{m}$ ),  $t_f$  the thickness of the graphene film ( $\sim 0.34 \text{ nm}$ ), and  $r_c$  the curvature radius. In addition, it is noted that, in this work, all transmittances of THz wave through the flexible modulator have been normalized to the reference signal of air.

The modulation performance of flexible THz modulator was studied in detail. The normalized intensities of THz wave through the modulator are plotted in **Figure 6(a)–(c)** in the flat, convex, and concave conditions, respectively. As shown in **Figure 6(a)**, significant modulation changes in THz transmission can be obtained by applying gate bias between  $-3$  and  $+3$  V when the modulator is in the flat condition. From **Figure 6(a)**, it can be observed that the transmittance has a maximum value of 81.3% at 1 V and a minimum value of 63.1% at  $-3$  V. Therefore, the MD of the modulator is calculated to be 22.4%. Importantly, when the graphene modulator is in the convex and concave conditions, the modulation depths estimated from **Figures 6(b)** and **(c)** are 21.3 and 21.4%, respectively, which are very close to that

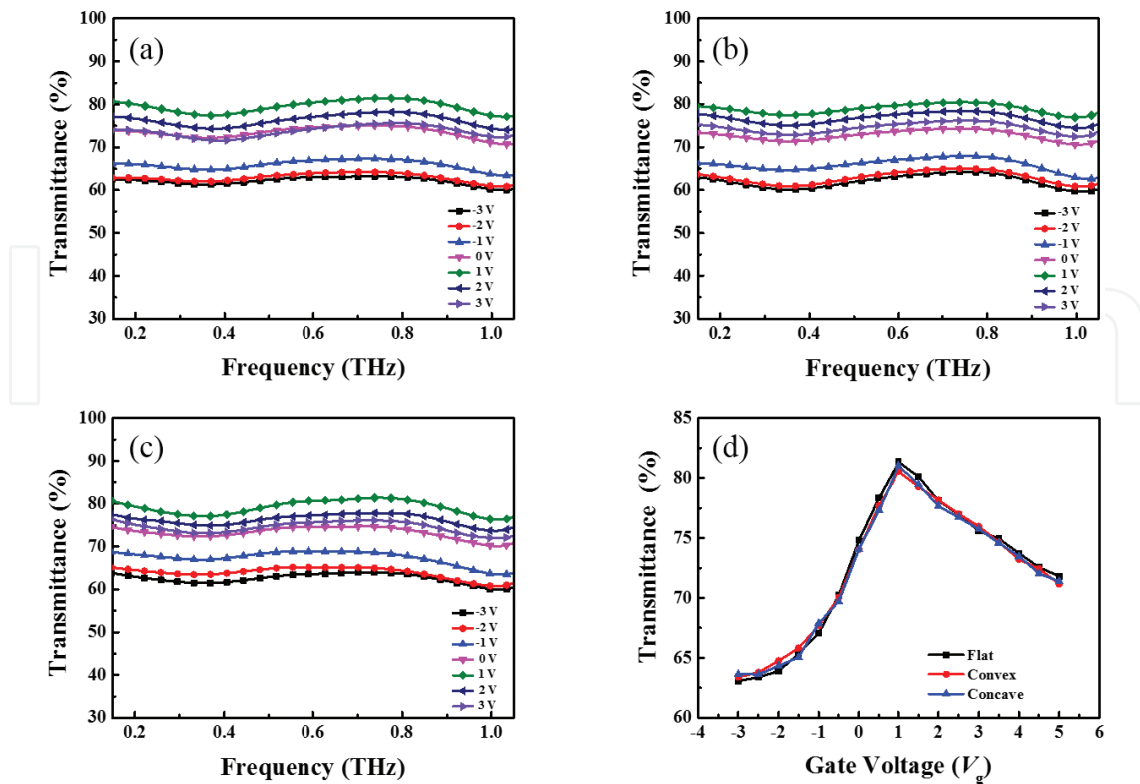


**Figure 6.** Normalized THz transmittance from the flexible graphene modulator as a function of frequency in the (a) flat, (b) convex, and (c) concave conditions at the fixed gate voltages ranging from  $-3$  to  $3$  V, with  $1$  V increment. (d) Normalized THz transmittances as a function of gate voltage from  $-3$  to  $5$  V at  $0.8$  THz in the flat, convex, and concave conditions.

in the flat condition. The performances of modulation under flat case, convex, and concave conditions are compared, as shown in **Figure 6(d)**. It can be observed that the three curves of transmittance-dependent gate bias at  $0.8$  THz are almost coincident. It indicates that the flexible modulator has excellent flexible performance, as the THz intensity modulation performances are steady under different bending deformations.

Further demonstrating the flexible performance of our THz graphene modulator, the repeatability has been studied by performing 1000 bending times. It shows that the THz intensity can still be effectively modulated by electrical gating. The modulation depths are 21.7, 21.1, and 20.5% at  $0.8$  THz in the flat, convex, and concave conditions, respectively, which are very close to that of the graphene modulator before bending. The curves of transmittances as a function of gate voltage at  $0.8$  THz before and after bending the graphene modulator 1000 times are nearly coincident, showing its high repeatability. We can conclude that the THz intensity modulation can be maintained not only in the bending condition but also after the long bending times, indicating superior flexible performance of the THz graphene modulator.

More importantly, a low insertion loss of THz wave was observed in our flexible THz modulator. By using air as the reference, the transmittance of the flexible modulator at  $1$  V gate voltage was measured and normalized, as plotted in **Figure 7**. It shows a broadband transmittance with the insertion loss less than  $1.2$  dB in the range of  $0$ – $1$  THz, which is much smaller

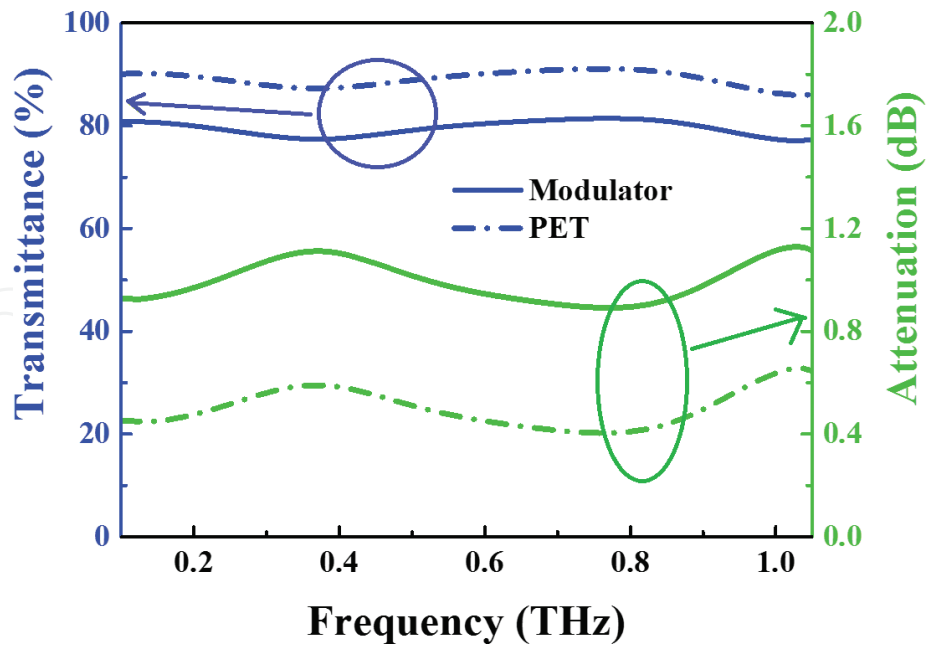


**Figure 7.** Transmittance and attenuation as a function of frequency for flexible graphene modulator at the gate voltage of 1 V (Dirac point) and PET.

than that of the Si substrate-based rigid graphene modulators (~5 dB) [52]. The extremely low loss can be attributed to the small refractive index of PET (1.65) as compared to that of Si (3.42). Our results indicate that employing a substrate with low refractive index is beneficial for obtaining a THz modulator with low insertion loss.

Modulation depth is one of the crucial parameters that determine the real applications of THz modulators. The typical MD of existing GFET modulators is only 20%. High MD has been achieved by a complex and exquisite integration of GFET with THz quantum cascade lasers

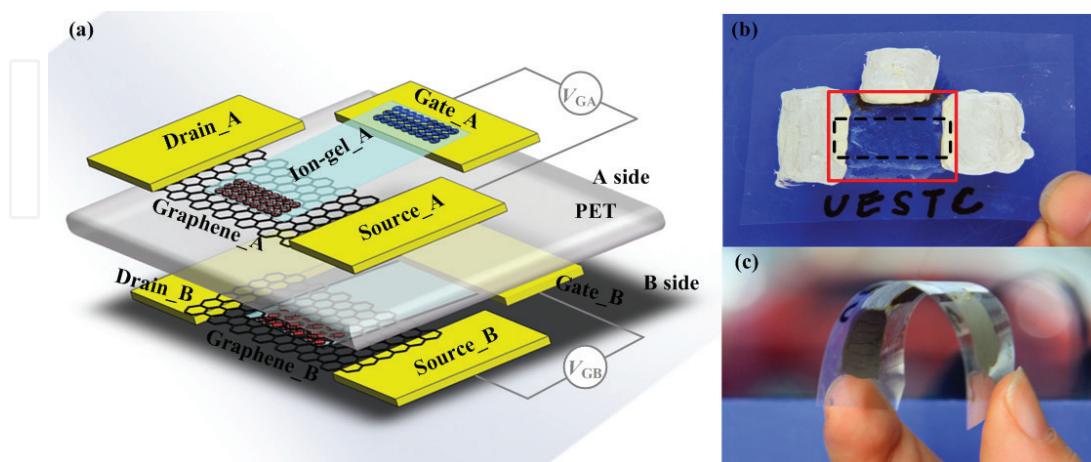


**Figure 8.** Overview of the cascaded THz modulators. (a) Schematic illustration of the device with cascaded two GFETs on a single PET substrate. (b) Photograph of the devices. The boundaries of graphene channel and ion-gel layer are marked with dark dotted lines and red solid lines, respectively. (c) Optical image showing the flexible nature of the device.

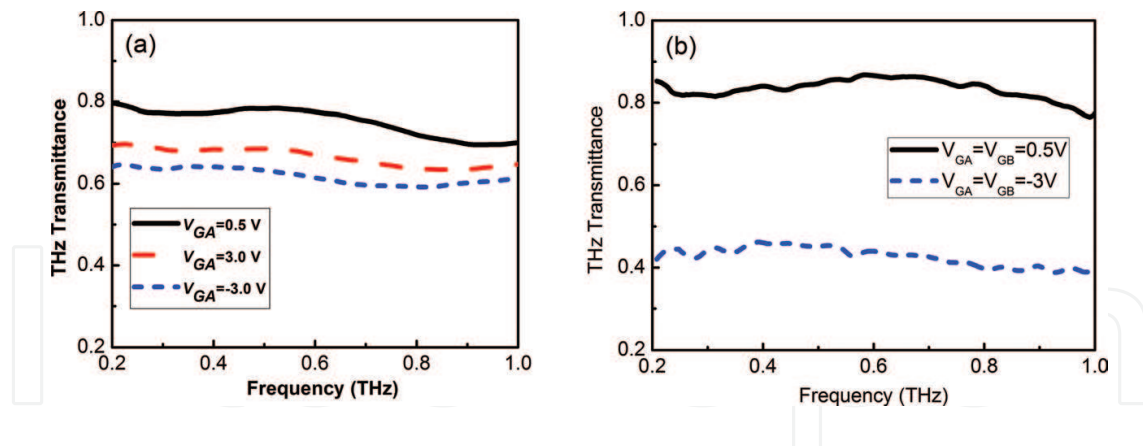


**Figure 9.** Normalized THz transmittance spectra of cascaded modulators under different gating schemes. Gate voltage applied to (a) single modulator and (b) dual modulators.

(QCL), despite the intrinsic MD of GFET is only 11% [53]. Inspired by the flexible and low-loss PET-GFET we developed previously, here, we propose an effective method to enhance the modulation depth by cascading multiple PET-GFET modulators with little sacrifice of insertion loss. Two GFETs were simultaneously fabricated on both sides of PET substrate to form a cascaded THz modulator, as shown in **Figure 8(a)**. The obtained devices are optically transparent and highly flexible, as shown in **Figure 8(b)** and **(c)**.

Modulation depth and insertion loss, two critical parameters of THz modulators are investigated. To investigate the modulation of the cascaded device, the THz transmittance was measured with an optimized gating scheme. **Figure 9** shows the transmission intensity of the THz waves through the graphene modulators at the frequency from 0.2 to 1.0 THz, which is normalized to the spectrum of air. Broadband modulation is obtained across the whole spectrum. When gate voltage is only applied to one modulator (**Figure 9(a)**), the transmittance at 0.6 THz reaches the maximum of 77.56% at 0.5 V and minimum of 61.41% at  $-3.0\text{ V}$ , respectively, leading to an MD of 20.8%. Maximum modulation depth was obtained when gate electrodes of both modulators were simultaneously driven. An enhanced MD of  $\sim 51\%$  is achieved with an IL of only 1.4 dB. To our best knowledge, this is the largest MD reported for flexible and broadband THz modulators and can be further improved by stacking more similar structures.

## 5. Conclusion

Field-effect transistors are one of the most widely discussed applications of graphene in micro-electronics and opto-electronics. However, graphene is intrinsically a zero-band-gap semiconductor, which is believed to be unsuitable for use in an electronic transistor. Fortunately, graphene FET finds its potential usage as THz modulators since THz wave is highly sensitive to the free carrier concentration, which can be effectively tuned by electrical gating in a graphene FET. In this chapter, the physics principle, device structure, and the modulation characteristics of GFET-based THz modulators, both rigid and flexible, are discussed

and experimentally demonstrated. It shows that THz modulators can be easily realized with graphene FET, and highly desired properties can be obtained such as the large modulation depth, high speed, broad width band, and insert loss.

## Acknowledgements

Supported by International Science & Technology Cooperation Program under Grant No. 2015DFR50870, Science Challenge Project under Grant No. TZ2018003, National Natural Science Foundation of China under grant No. 51572042, and Sichuan Science and Technology projects under Grant No. 2014GZ0091, 2015GZ0069, 2014GZ0003.

## Conflict of interest

The authors declare no conflict of interest.

## Author details

Qi-Ye Wen<sup>1\*</sup>, Yu-Lian He<sup>1</sup>, Jing-Bo Liu<sup>2</sup>, Qi Mao<sup>2</sup>, Qing-Hui Yang<sup>1</sup>, Zhi Chen<sup>3</sup> and Huai-Wu Zhang<sup>1</sup>

\*Address all correspondence to: qywen@163.com

1 State Key Laboratory of Electronic Thin Films and Integrated Devices, University of Electronic Science and Technology of China, Chengdu, Sichuan, PR China

2 School of Electrical Engineer and Intelligentization, Dongguan University of Technology, Dongguan, Guangdong Province, PR China

3 National Key Laboratory of Science and Technology of Communication, University of Electronic Science and Technology of China, Chengdu, PR China

## References

- [1] Chan WL, Deibel J, Mittleman DM. Imaging with terahertz radiation. *Reports on Progress in Physics*. 2007;**70**:1325-1379
- [2] Jepsen PU, Cooke DG, Koch M. Terahertz spectroscopy and imaging, modern techniques and applications. *Laser & Photonics Reviews*. 2011;**5**:124-166
- [3] Kleine-Ostmann T, Nagatsuma T. A review on terahertz communications research. *Journal of Infrared, Millimeter, and Terahertz Waves*. 2011;**32**:143-171

- [4] Ho L, Pepper M, Taday P. Terahertz spectroscopy: Signatures and fingerprints. *Nature Photonics*. 2008;**2**:541-543
- [5] Chen HT, Padilla WJ, Zide JMO. Active terahertz metamaterial devices. *Nature*. 2006;**444**:597-600
- [6] Rahm M, Li JS, Padilla WJ. THz wave modulators: A brief review on different modulation techniques. *Journal of Infrared, Millimeter, and Terahertz Waves*. 2013;**34**:1-27
- [7] Ostmann TK, Dawson P, Pierz K. Room temperature operation of an electrically driven terahertz modulator. *Applied Physics Letters*. 2004;**84**:3555-3557
- [8] Shrekenhamer D, Rout S, Strikwerda A C. High speed terahertz modulation from metamaterials with embedded high electron mobility transistors. *Optics Express*. 2011;**19**:9968-9975
- [9] Chan WL, Chen HT, Taylor AJ. A spatial light modulator for terahertz beams. *Applied Physics Letters*. 2009;**94**:213511
- [10] Chen HT, Padilla WJ, Cich MJ. A metamaterial solid-state terahertz phase modulator. *Nature Photonics*. 2009;**3**:148-151
- [11] Chen HT, Padilla WJ, Zide JMO. Ultrafast optical switching of terahertz metamaterials fabricated on ErAs/GaAs nanoisland superlattices. *Optics Letters*. 2007;**32**:1620-1622
- [12] Chen HT, Yang H, Singh R. Tuning the resonance in high temperature superconducting terahertz metamaterials. *Physical Review Letters*. 2010;**105**:247402
- [13] Jin BB, Zhang CH, Engelbrecht S. Low loss and magnetic field-tunable superconducting terahertz metamaterial. *Optics Express*. 2010;**18**:17504-17509
- [14] Wen QY, Zhang HW, Yang QH. Terahertz metamaterials with VO<sub>2</sub> cut-wires for thermal tenability. *Applied Physics Letters*. 2010;**97**:021111
- [15] Xiong Y, Wen QY, Chen Z. Tuning the phase transitions of VO<sub>2</sub> thin films on silicon substrates using ultrathin Al<sub>2</sub>O<sub>3</sub> as buffer layers. *Journal of Physics D: Applied Physics*. 2014;**47**:455304
- [16] Alius H, Dodel G. Amplitude-, phase-, and frequency modulation of far-infrared radiation by optical excitation of silicon. *Infrared Physics*. 1991;**32**:1-11
- [17] Vogel T, Dodel G, Holzhauer E. High-speed switching of far-infrared radiation by photoionization in a semiconductor. *Applied Optics*. 1992;**31**:329-337
- [18] Okada T, Tanaka K. Photo-designed terahertz devices. *Scientific Reports*. 2011;**1**:121
- [19] Cheng LJ, Liu L. Optical modulation of continuous terahertz waves towards cost-effective reconfigurable quasi-optical terahertz components. *Optics Express*. 2013;**21**:28657-28667
- [20] Xie ZW, Wang XK, Ye JS. Spatial terahertz modulator. *Scientific Reports*. 2013;**3**:3347

- [21] Wen TL, Zhang DN, Wen QY. Enhanced optical modulation depth of terahertz waves by self-assembled monolayer of plasmonic gold nanoparticles. *Advanced Optical Materials*. 2016;**4**:1974-1980
- [22] Weis P, Garcia-Pomar JL, Hoh M. Spectrally wide-band terahertz wave modulator based on optically tuned graphene. *ACS Nano*. 2012;**6**:9118-9124
- [23] Wen QY, Tian W, Mao Q. Graphene based all-optical spatial terahertz modulator. *Scientific Reports*. 2014;**4**:7409
- [24] Zhang B, He TT, Shen JL. Conjugated polymer-based broadband terahertz wave modulator. *Optics Letters*. 2014;**39**:6110-6113
- [25] Shi ZW, Cao XX, Wen QY. Terahertz modulators based on silicon nanotip array. *Advanced Optical Materials*. 2018;**6**:1700620
- [26] Kannegulla A, Shams MIB, Liu L. Photo-induced spatial modulation of THz waves opportunities and limitations. *Optics Express*. 2015;**23**:32098-32112
- [27] Driscoll T, Kim HT, Chae BG. Memory metamaterials. *Science*. 2009;**325**:5947
- [28] Driscoll T, Palit S, Qazilbash MM. Dynamic tuning of an infrared hybrid-metamaterial resonance using vanadium dioxide. *Applied Physics Letters*. 2008;**93**:024101
- [29] Seo M, Kyoung J, Park H. Active terahertz nanoantennas based on VO<sub>2</sub> phase transition. *Nano Letters*. 2010;**10**(6):2064-2068
- [30] Goldam MD, Driscoll T, Chapler B. Reconfigurable gradient index using VO<sub>2</sub> memory metamaterials. *Applied Physics Letters*. 2011;**99**:044103
- [31] Shi QW, Huang WX, Zhang YX. Giant phase transition properties at terahertz range in VO<sub>2</sub> films deposited by sol-gel method. *ACS Applied Materials & Interfaces*. 2011;**3**(9):3523-3527
- [32] Kyoung J, Seo M, Park H. Giant nonlinear response of terahertz nanoresonators on VO<sub>2</sub> thin film. *Optics Express*. 2010;**18**(16):16452-16459
- [33] Castro Neto AH, Guinea F, Peres NMR. The electronic properties of graphene. *Reviews Modern Physics*. 2009;**81**:109-162
- [34] Zhong MY, Xu DK, Yu XG. Interface coupling in graphene/fluorographene heterostructure for high-performance graphene/silicon solar cells. *Nano Energy*. 2016;**28**:12-18
- [35] Akinwande D, Tao L, Yu Q. Large-area graphene electrodes: Using CVD to facilitate applications in commercial touchscreens, flexible nanoelectronics, and neural interfaces. *IEEE Nanotechnology Magazine*. 2015;**9**(3):6-14
- [36] Han MY, Ozyilmaz B, Zhang Y. Energy band-gap engineering of graphene nanoribbons. *Physical Review Letters*. 2007;**98**:206805
- [37] Chen Z, Lin YM, Rooks MJ. Graphene nano-ribbon electronics. *Physica E: Low-dimensional Systems and Nanostructures*. 2007;**40**:228

- [38] Sensale-Rodriguez B, Yan R, Kelly MM. Broadband graphene terahertz modulators enabled by intraband transitions. *Nature Communications*. 2012;**3**:780
- [39] Maeng I, Lim S, Chae SJ. Gate-controlled nonlinear conductivity of Dirac fermion in graphene field-effect transistors measured by terahertz time-domain spectroscopy. *Nano Letters*. 2012;**12**:551
- [40] Liao L, Bai J, Qu Y. Single-layer graphene on Al<sub>2</sub>O<sub>3</sub>/Si substrate: Better contrast and higher performance of graphene transistors. *Nanotechnology*. 2010;**21**:15705
- [41] Gronera MD, Elama JW, Fabreguette FH. Electrical characterization of thin Al<sub>2</sub>O<sub>3</sub> films grown by atomic layer deposition on silicon and various metal substrates. *Thin Solid Film*. 2002;**413**:186
- [42] Li X, Cai W, An J. Large-area synthesis of high-quality and uniform graphene films on copper foils. *Science*. 2009;**324**:1312
- [43] Liu JB, Li PJ, Chen YF. Large-area synthesis of high-quality and uniform monolayer graphene without unexpected bilayer regions. *Journal of Alloys Compounds*. 2014;**615**:415-418
- [44] Malard LM, Pimenta MA, Dresselhaus G. Raman spectroscopy in graphene. *Physics Reports*. 2009;**473**:51
- [45] Ferrari AC, Meyer JC, Scardaci V. Raman spectrum of graphene and graphene layers. *Physical Review Letters*. 2006;**97**:187401
- [46] Liang X, Sperling BA, Calizo I. Toward clean and crackless transfer of graphene. *ACS Nano*. 2011;**5**:9144-9153
- [47] Schwierz F. Graphene transistors. *Nature Nanotechnology*. 2010;**5**:487
- [48] Konar A, Fang T, Jena D. Effect of high-K gate dielectrics on charge transport in graphene-based field effect transistors. *Physical Review B*. 2010;**82**:15452
- [49] Tao H, Bingham CM, Strikwerda AC. Highly flexible wide angle of incidence terahertz metamaterial absorbers: Design, fabrication, and characterization. *Physical Review B*. 2008;**78**:241103
- [50] Wang ZG, Chen YF, Li PJ. Flexible graphene-based electroluminescent devices. *ACS Nano*. 2011;**5**:7149-7154
- [51] Mao Q, Wen QY, Tian W. High-speed and broadband terahertz wave modulators based on large-area graphene field-effect transistors. *Optics Letters*. 2014;**39**:5649-5652
- [52] Liang G, Hu X, Yu X. Integrated terahertz graphene modulator with 100% modulation depth. *ACS Photonics*. 2015;**2**:1559-1566
- [53] Liu JB, Li PJ, Chen YF. Flexible terahertz modulator based on coplanar-gate graphene field-effect transistor structure. *Optics Letters*. 2016;**41**:816-819.1

